Two-dimensional nonlinear dynamics of four driven vortices

P. N. Guzdar, J. M. Finn, A. V. Rogalsky, and J. F. Drake
Institute for Plasma Research, University of Maryland, College Park, Maryland 20742
(Received 4 October 1993)

The interaction of four alternately driven counterrotating vortices in a two-dimensional box, with inpenetrable free-slip boundary conditions in the x direction and periodic boundary conditions in the y direction, has been studied numerically. For viscosity above a critical value the nonlinear state consists of four alternately counterrotating vortices. For a lower value of the viscosity the system evolves to a nonlinear steady state consisting of four vortices and shear flow generated by the "peeling instability" [Drake *et al.*, Phys. Fluids B **4**, 447 (1992)]. For a still lower viscosity the steady-state nonlinear state undergoes a Hopf bifurcation. The periodic state is caused by a secondary instability associated with vortex pairing. However, the vorticity of the shear flow, though periodic, has a definite sign. With a further decrease in the viscosity, a global bifurcation gives rise to a periodic state during which the vorticity of the shear flow changes sign. At even lower viscosity, there is a transition to a steady state, involving dominantly shear flow and a two-vortex state. Finally, this state undergoes a bifurcation to a temporally chaotic state, with the further decrease of viscosity. The results are compared to some recent experiments in fluids with driven vortices [P. Tabeling *et al.*, J. Fluid Mech. **215**, 511 (1990)].

PACS number(s): 47.15.Gf, 47.20.Ky, 47.20.Ft, 47.27.Pa

I. INTRODUCTION

Generation of convective cells in fluids and plasmas is a ubiquitous phenomenon. In environments as diverse as the turbulent sun [1], on one hand, and a simple heated fluid in a laboratory [2] in the presence of gravity, on the other, Rayleigh-Bénard convection cells are readily driven. The nonlinear fate of these cells is, however, dependent on the details of the geometry and the value of the dimensionless parameters, such as the Rayleigh number, the Prandtl number, and the elongation of the vortices for the fluid in question. However, the nonlinear evolution causes drastic local modification of the source of the instability, namely, the temperature gradient, leading to a complex interplay between the nonlinear mode coupling and the source modification. There are, however, comparatively simpler physical systems, in which the source is unaltered by the nonlinear evolution. For such systems, the nonlinear evolution is dominated by mode coupling rather than profile or source modification. The present work is motivated by these systems.

The simpler systems referred to above are those in the experiments reported in [3–7], in which a periodic array of alternate, counterrotating, two-dimensional vortices are driven by electromagnetic forcing. By passing a current through a cell containing a normal solution of sulfuric acid and an array of permanent magnets of alternating polarity at the bottom of the cell, the Lorentz force stirs the fluid, producing the vortices. The two dimensionality of the flow is ensured by restricting the thickness of the fluid.

The basic results of the experiments for four counterrotating vortices can be summarized as follows. At low currents, which corresponds to weak forcing and hence low Reynolds number, the flow is a linear array of counterrotating vortices [4]. This stable state becomes unstable beyond a critical current. The linear array is now comprised of nonuniform tilted vortices, alternately large and small. A further increase in the current enhances the tilt and makes the large vortices larger and the alternate smaller vortices even smaller. A further increase in the current leads to a state with half the number of corotating vortices as compared to the initial state. Beyond this point, any increase of the current leads to time-dependent states [5]. First a supercritical Hopf bifurcation occurs. At a value of the current equal to three times the value when the Hopf bifurcation occurred, a sequence of period-doubling bifurcations occurs, followed by a transition to temporal chaos.

In recent papers [8,9], an analytic as well as numerical study of two driven, counterrotating vortices was undertaken. It was shown that for large viscosity (or weak forcing) the nonlinear state was comprised of two periodic counterrotating vortices. A decrease in the viscosity led to an instability that caused the vortices to tilt. Also, one vortex was larger than the other. The cause of the tilt was an instability that generated shear flow. The larger vortex had the same vorticity as the shear flow, while the smaller one was counterrotating. A further decrease in the viscosity led to a state in which only a single vortex survived and was embedded in shear flow. A further decrease in the viscosity only led to a decrease in the size of the single vortex, relative to the strength of the shear flow. All the nonlinear states were time independent.

In the present work we have studied the stability and nonlinear evolution of four driven, alternately counterrotating vortices. We present the equations and a brief description of the numerical scheme used in our investigation in Sec. II. In Sec. III the analytical and numerical results are presented. Finally in Sec. IV we compare our results to those of the experiments.

 ©1994 The American Physical Society

II. BASIC EQUATIONS

The two-dimensional isothermal Navier-Stokes equations are used. They are

$$\frac{\partial \rho}{\partial t}+\nabla\cdot(\rho\mathbf{v})=0 \tag{1}$$

and

$$\frac{\partial}{\partial t}(\rho\mathbf{v})+\nabla\cdot(\rho\mathbf{v}\mathbf{v})=-c_s^2\nabla\rho+\nu\nabla^2\mathbf{v}+\mathbf{F}\ , \tag{2}$$

where $\mathbf{F}$ is an external forcing function, ρ is the mass density, c_s is the speed of sound, and ν is the viscosity. The boundary conditions are periodic in y with period L_y and impenetrable, free-slip conditions at $x=0$ and L_x, i.e., $v_x=0$ and $\partial v_y/\partial x=\partial\rho/\partial x=0$. The two-dimensional code we have used for the present study was developed for the earlier work reported in [8,9]. Incompressibility ($\nabla\cdot\mathbf{v}=0$) is ensured by making $v/c_s<1$ such that ρ remains nearly constant in space and time, if initially it is assumed to be uniform. As a consequence the velocity can be written in terms of a stream function as $\mathbf{v}=-\nabla\phi\times\mathbf{z}$ and the equation for the vorticity is $\omega=\mathbf{z}\cdot\nabla\times\mathbf{v}$,

$$\frac{\partial\omega}{\partial t}+\mathbf{v}\cdot\nabla\omega=\mu\nabla^2\omega+S\ , \tag{3}$$

where $\mu=\nu/\rho$ and $S=(1/\rho)\nabla\times\mathbf{F}$. The flow remains in equilibrium for $S=\mu\lambda^4\phi$, where $\lambda^2=(2\pi)^2(1/L_x^2+16/L_y^2)$.

In our present work the length scales are normalized to L_x and the time scales are normalized to L_x/c_s. The normalized viscosity is μ/c_sL_x, and $|\mathbf{v}|^{\max}$, the maximum value of the x velocity for the initial equilibrium flow, is chosen to be equal to $0.1c_s$. We hasten to remind the reader that the Reynolds number is not $|\mathbf{v}|^{\max}L_x/\mu$. This is because the maximum velocity that develops in the simulation is much lower than the initial velocity $0.1c_s$ and systematically decreases with the decrease in viscosity. Also the acoustic velocity is used merely for the purpose of normalization and does not in any way influence the results presented in this paper. It appears because we are using the compressible equations (1) and (2) (though ensuring incompressibility as mentioned above) rather than the incompressible vorticity equation (3). Although the compressible equations require a smaller time step (a factor of 10 for $v/c_s=0.1$) compared to solving Eq. (3), they have the advantage of being completely vectorizible. Also they do not have the disadvantage, as do the incompressible equations, of having to solve a Poisson equation to obtain ϕ from ω.

III. NUMERICAL RESULTS

We now discuss the results obtained using our numerical code. There are basically two dimensionless parameters in the problem: L_y and μ. $L_y=2.0$ has been chosen for all the results presented in this paper. We have focused on investigating the change in dynamical behavior of the four vortices as we vary the viscosity. For most of the runs, the number of grid points in the x direction is $n_x=31$ and the number in the y direction is $n_y=61$. For the lower viscosity runs we have increased the spatial resolution by a factor of 2 to ensure that the results are not affected by the grid size. The scalar potential for the four vortex case can be written as

$$\phi=\phi_0\sin(\pi x)\sin(2\pi y/L_y)\ . \tag{4}$$

In Fig. 1(a) we show the stream function and the vorticity for $\mu=10^{-2}$. There are four alternately counterrotating vortices in steady state. The vortices are of equal strength. The vorticity contours are identical to the stream function contours. As the viscosity is reduced to 4.2×10^{-3} [Fig. 1(b)], an instability develops which leads to the generation of shear flow. The consequence of this flow is that the vortices are tilted and those which have the same vorticity as the shear flow are now larger than those with the opposite vorticity. The generation of this flow has been studied in detail in Refs. [8] and [9]. As found earlier, the instability is inviscid or dissipative depending on the elongation of the vortices. The inviscid growth rate for the generation of shear flow by $2m$ alternately counterrotating vortices is

$$\hat{\gamma}=\frac{3[m^2-L_y^2]}{4[m^2+L_y^2]}\ , \tag{5}$$

where γ is the normalized growth rate, which is defined as $\gamma L_y/4\pi^2\phi_0$. The perturbations used in obtaining this dispersion relation were assumed to have a time dependence given by $\exp(\gamma t)$. This is a straightforward extension of the four-mode theory given in Refs. [8] and [9]. For the four-vortex case, $m=2$ and since $L_y=2$, the inviscid mode is marginally stable. Thus the instability we observe occurs only in the presence of viscosity, because small yet finite viscosity relaxes the constraint of perfect conservation of vorticity. Again a theory based

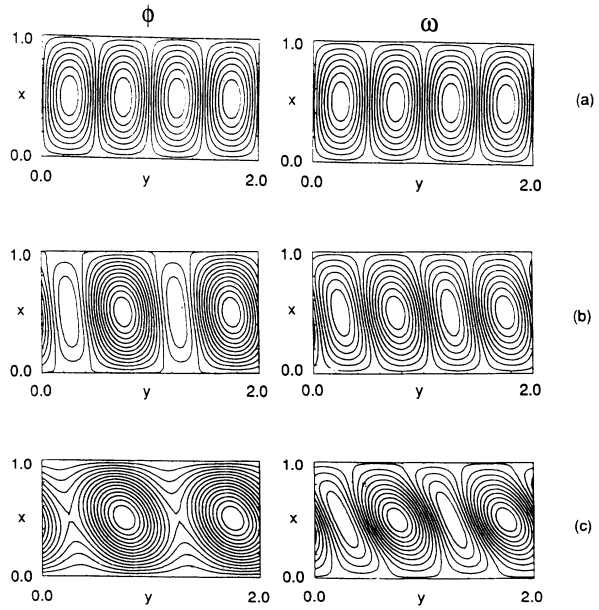

FIG. 1. Contours of the stream function and vorticity for (a) $\mu=10^{-2}$, (b) $\mu=4.2\times10^{-3}$, and (c) $\mu=3\times10^{-3}$.

on the four-mode model with viscosity, of Ref. [9] [Eq. (11)], can readily yield the growth for the viscous mode. We remind the reader that the validity of the truncation to four modes is ensured only for ideal modes or for viscous modes with large viscosity. By large viscosity we mean those values of viscosity for which the dissipation scale lengths are comparable to the box size. A further reduction in the viscosity down to a value of $\mu=3.0\times10^{-3}$ [Fig. 1(b)] causes the shear flow to increase. Also the smaller vortices are completely absent. The contours for the stream function in Fig. 1(c) show that there are half as many vortices as the initial state and these are corotating. As discussed in detail in our earlier work, once the counterrotating four-vortex solutions become unstable to the shear flow, the O point associated with the smaller vortices bifurcates into an X point and two smaller O points which are rapidly dissipated at the boundary leaving two O points and two X points which are responsible for the island structure seen in Figs. 1(b) and 1(c). As a consequence the size of these islands in the periodic direction is twice the size of the initial vortices. Again these results are in agreement with the earlier two-vortex study (Refs. [8] and [9]) and with the experimental observations reported in Ref. [5].

What determines the sign of the vorticity of the shear flow? In the results presented above, a small seed for the shear flow was introduced initially. Had we chosen a seed with the opposite parity the vortices would have been tilted by the shear flow with negative vorticity. Thus there are two degenerate states, one for which the shear flow has positive vorticity and one for which the vorticity is negative. Since the equations and boundary conditions are symmetric, about $x=\frac{1}{2}$, in the absence of a seed, the symmetry breaking would occur through machine noise or a finite difference scheme which does not preserve the symmetry inherent in the equations.

So far the results are similar to the earlier results for the two-vortex case, the only difference being that in this study there are four counterrotating vortices instead of two. In the two-vortex case [9] any further reduction in the viscosity leads to a decrease in the island width and an increase in the relative strength of the shear flow. In fact, at very low viscosity the presence of the vortex island is hardly discernible in the contour plots for the stream function. However, for the four-vortex case the behavior is very different for viscosity lower than 3.0×10^{-3}. In Figs. 2(a)–2(c) we show the stream function and the vorticity at three different instants of time for $\mu=2.75\times10^{-3}$. The first frame shows the initial condition ($t=0$). The second frame at $t=1000$ shows the state very similar to that in Fig. 1(c), where two tilted corotating vortices embedded in a shear flow are in steady state. However, after a significant time a secondary instability develops which causes the system to evolve to a state having an admixture of four- and two-vortex, and shear flow. The secondary instability is the well-known pairing instability [10–12] of corotating vortices. In the two-vortex case this secondary instability cannot occur. This instability requires at least two corotating cells, and in the two-vortex case there is only one such cell in the periodic box. For point vortices of equal

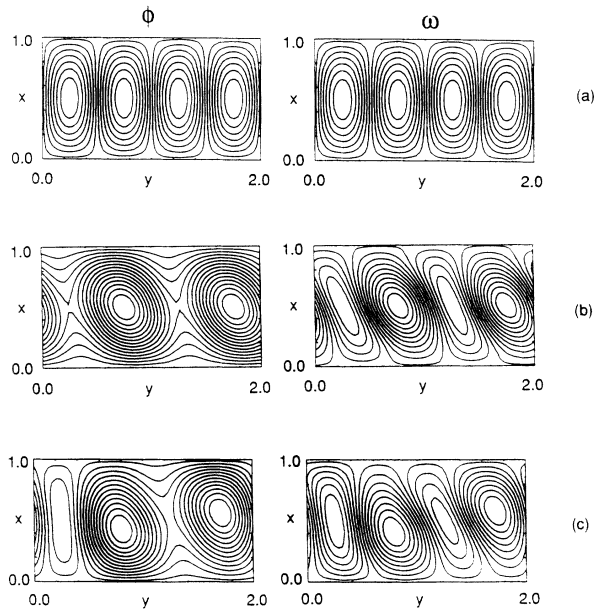

FIG. 2. Contours of the stream function and vorticity for $\mu=2.75\times10^{-3}$ at (a) $t=0$, (b) $t=1000$, and (c) $t=8000$.

strength the pairing instability leads to a rotation of the vortices around the common vorticity centroid [10]. However, in the present case, since the vortices are of finite size, there is also the possibility of merging or coalescence of the vortices [11,12]. This merging can happen if the distance between the centroids of the two vortices is smaller than a certain critical distance [12]. For two isolated symmetric vortices once the merging is initiated the final state corresponds to a single symmetric vortex. However, in the present case we have additional driving, as well as finite viscosity which can influence the final state. Thus the final state observed in Fig. 2(c) at $t=8000$ is one in which the centroids of the two vortices have rotated by a small amount and a little merging has occurred. This is a new steady state or fixed point. The merging of the two corotating vortices is clearly seen on the contours for the stream function. Also the centroids of each vortex is no longer at $x=\frac{1}{2}$. The centroid of the left vortex is below $x=\frac{1}{2}$, while the centroid of the right vortex is above $x=\frac{1}{2}$. Another interesting aspect of the secondary instability is seen by comparing the stream functions in Figs. 2(b) and 2(c). The open streamlines at the top and bottom indicate the presence of shear flow. In Fig. 2(c) we observe that the open streamlines in Fig. 2(b) have reconnected causing the coalescence of the two corotating vortices. Thus there is a reduction and hence stabilization of the shear flow by the secondary coalescence instability. Actually there are four such degenerate fixed points because of the symmetry in the system. If we recall that the system is periodic in the y direction, then pairing an occur between the right vortex and the left vortex in the adjoining periodic box to the right, or the left vortex and the right vortex in the same box. This basically corresponds to a change of the phase in the stream function. Furthermore there are also two similar states

for which the shear flow has a negative vorticity.

In Fig. 3 we show the time history of various Fourier components of the stream function. In Fig. 3(a) we show the shear flow. The $\sin(2\pi y/L_y)$ (S) and $\cos(2\pi y/L_y)$ (C) components are shown in Fig. 3(b). Finally in Fig. 3(c), the $\sin(4\pi y/L_y)$ and $\cos(4\pi y/L_y)$ are plotted as a function of time. Initially the shear flow grows rapidly and the driven component of the four-vortex decreases and a "steady state" is reached. However, at $t=1500$ a secondary instability, generating the subharmonic components corresponding to $\sin(2\pi y/L_y)$ and $\cos(2\pi y/L_y)$ components, begins to grow. The pairing instability, which causes the two vortices to rotate around each other, generates the subharmonic components. This in turn suppresses the shear flow. The suppression of the shear flow causes the four-vortex component to increase.

Thus up to this stage we have encountered seven equilibrium states. First we have a pure four-vortex state for $\mu \leq 5.0\times10^{-3}$. Then two degenerate states with shear flow and four-vortex equilibria exist for $3.0\times10^{-3} \leq \mu \leq 5.0\times10^{-3}$. Finally there are four degenerate states involving an admixture of shear flow, two-vortex, and four-vortex equilibria for $2.5\times10^{-3} \leq \mu \leq 3.0\times10^{-3}$. The various transitions that we have encountered are equilibrium pitchfork bifurcations. They are shown schematically in Fig. 4.

Now a decrease in the viscosity to $\mu=2.25\times10^{-3}$ leads to a supercritical Hopf bifurcation. Shown in Fig. 5 are the various Fourier harmonics as a function of time. In the earlier phase, $t<200$, the primary instability is that associated with the generation of shear flow. This is followed again by a secondary instability causing pairing of the two corotating vortices. This instability, which leads to the excitation of $k_y=2\pi y/L_y$ [Fig. 5(b)], again causes a strong suppression of the shear flow Fig. 5(a). This again allows the driven four-vortex component to increase [Fig. 5(c)] and regenerate the shear flow. The pairing instability is again initiated and the cycle repeats.

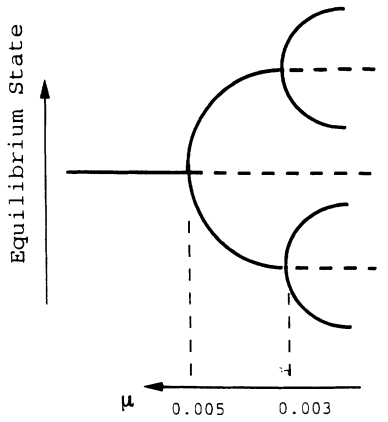

FIG. 4. Schematic of pitchfork bifurcation for $3.0\times10^{-3} \leq \mu \leq 2.0\times10^{-2}$.

Thus a periodic state emerges, which oscillates between the tilted four-vortex state and the corotating two-vortex state. In Fig. 6(a) we show the stream function contours for the tilted four-vortex state, when the shear flow is minimum at $t=950$. The two-vortex state, when the shear flow is maximum, is shown at $t=1050$ in Fig. 6(b). A further decrease in the viscosity to $\mu=2.1216\times10^{-3}$ leads to an increase in the amplitude of the oscillations of the various Fourier components (Fig. 7). What is perhaps most interesting to observe is that the shear flow almost becomes zero, yet remains positive. Also the period of the oscillation increases from $T=200$ for $\mu=2.25\times10^{-3}$ to $T=600$ for $\mu=2.1216\times10^{-3}$. The increase in the period occurs because as the shear flow gets closer to zero during its periodic excursion, the state is very similar to the initial state, which is a pure four-vortex state. As a consequence the period of the subsequent oscillations begins to approach the period of the first oscillation, which is $T=1000$. Thus at this point the oscillation is between almost a pure four-vortex state and

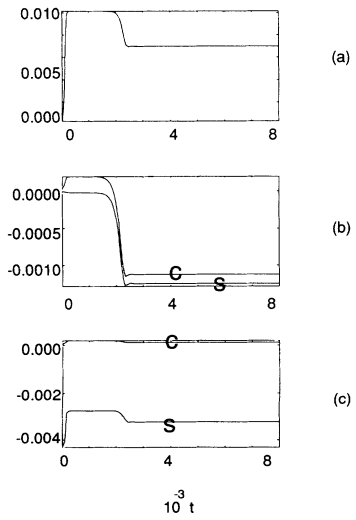

FIG. 3. For $\mu=2.75\times10^{-3}$, time history of the (a) $k_y=0$ Fourier component, sin (S) and cos (C) components for (b) $k_y=2\pi y/L_y$, and (c) $k_y=4\pi y/L_y$ for ϕ.

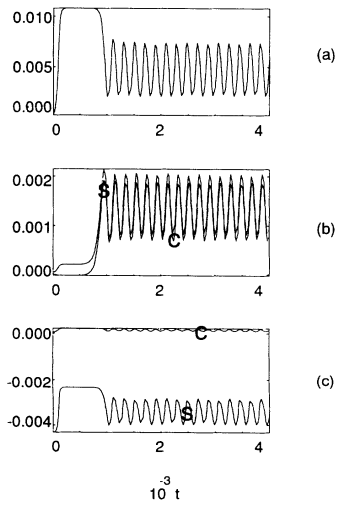

FIG. 5. For $\mu=2.25\times10^{-3}$, time history of the (a) $k_y=0$ Fourier component, sin (S) and cos (C) components for (b) $k_y=2\pi y/L_y$, and (c) $k_y=4\pi y/L_y$ of ϕ.

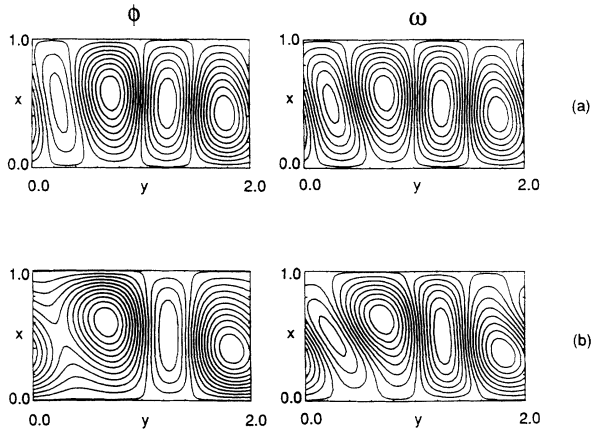

FIG. 6. Contours of the stream function at (a) $t=950$ and (b) $t=1050$ for $\mu=2.25\times10^{-3}$.

four-vortex with shear flow.

Perhaps the most dramatic bifurcation is a global bifurcation which occurs at $\mu=2.1213\times10^{-3}$. The shear flow *reverses* sign. In Fig. 8 we show the various Fourier harmonics. The significant difference for this case compared to the previous case in Fig. 7 is that the $\cos(2\pi y/L_y)$ and the $\sin(2\pi y/L_y)$ reverse phase. In Fig. 9 we show the stream function at $t=600$, 800, 960, 1080, 1120, and 1400 as the shear flow reverses. At $t=600$ [Fig. 9(a)], two tilted corotating vortices with shear flow, reminiscent of the earlier fixed point [Fig. 2(b)] is seen. The pairing instability that occurs later causes the two vortices to rotate around each other, as seen in Fig. 9(b). The vortex to the right has shifted below $x=\frac{1}{2}$, while the vortex to the left has moved above $x=\frac{1}{2}$. This rotation of the vortex pair leads to stabilization of the shear flow. As a consequence the driven four-vortex state begins to reemerge. At $t=960$ in Fig. 9(c), the four vertical, alternately counterrotating vortices have completely reemerged. However, the centroids of the second and fourth vortices are still displaced from $x=\frac{1}{2}$. The emerging four-vortex state, together with the residual two-vortex pair (characterized by centroids displaced from $x=\frac{1}{2}$), forces the emerging four-vortex state to have a tilt which seeds the shear flow with a sign opposite to the original seed, as clearly seen in Figs. 9(d) and 9(e). As a consequence at $t=1400$ [Fig. 9(f)] the state is similar to that at $t=600$; however, the shear flow has a vorticity which is opposite to that in Fig. 9(a). Once again the pairing instability occurs. However, the rotation of the corotating pair about the common centroid is now in a direction opposite to that in Fig. 9(b). As a consequence the emerging four-vortex state is forced to tilt and provide a seed for the shear flow instability in the direction similar to the initial one. This process repeats itself.

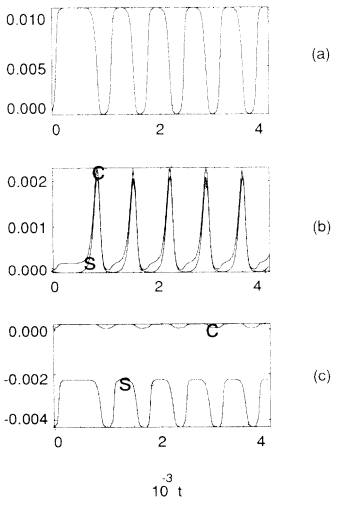

FIG. 7. For $\mu=2.1216\times10^{-3}$, time history of the (a) $k_y=0$ Fourier component, sin (S) and cos (C) components for (b) $k_y=2\pi y/L_y$, and (c) $k_y=4\pi y/L_y$ of ϕ.

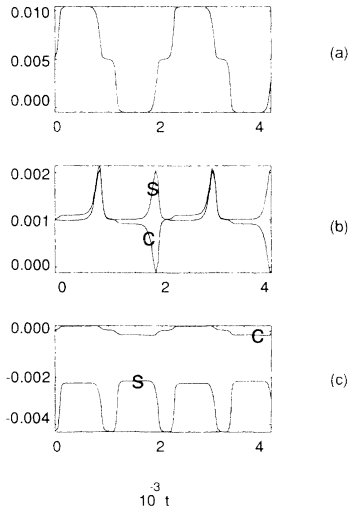

FIG. 8. For $\mu=2.1213\times10^{-3}$, time history of the (a) $k_y=0$ Fourier component, sin (S) and cos (C) components for (b) $k_y=2\pi y/L_y$, and (c) $k_y=4\pi y/L_y$ of ϕ.

This interesting global bifurcation can be schematically represented by the diagram in Fig. 10. We qualitatively illustrate it in a two-dimensional phase portrait, although the dynamics is clearly in a higher-dimensional space. The horizontal direction corresponds to the shear Fourier component and the vertical direction to the $\sin(2\pi y/L_y)$ component. Prior to the bifurcation there is an unstable point at the center consisting of a pure $4\pi y/L_y$ vortex flow without shear flow, and two stable limit cycles, with opposite shear flows [Fig. 10(a)]. The initial four-vortex state follows a trajectory which is attracted to one of the two limit cycles. After the bifurcation [Fig. 10(b)], a new stable orbit encircling the unstable equilibrium at the center is formed. The initial limit cycle crosses the stable manifold at the center to give rise to the new limit cycle [which looks like a figure eight in Fig. 10(b)]. Although we have schematically showed the bifurcation occurring in two dimensions, this global bifurcation occurs in the same way in higher dimension.

Now as we reduce the viscosity, the period of the oscillation keeps decreasing. However, at $\mu=1.0\times10^{-3}$, a

new phase to the pairing phenomenon occurs, causing the period of the oscillations to increase. This feature is more clearly seen at lower viscosity, hence we show this behavior for $\mu=7.5\times10^{-4}$. In the early phase, after the generation of the shear flow, the pairing phenomenon occurs as usual. This is readily seen on the various Fourier components in Fig. 11. As the viscosity is reduced to $\mu=7.3\times10^{-4}$ the period of the oscillation increases by a factor of 2 as seen in the various Fourier harmonics in Fig. 12. If one looks at the stream function [Fig. 13(a)] at $t=500$, the two corotating vortices have coalesced significantly. As a consequence the system has

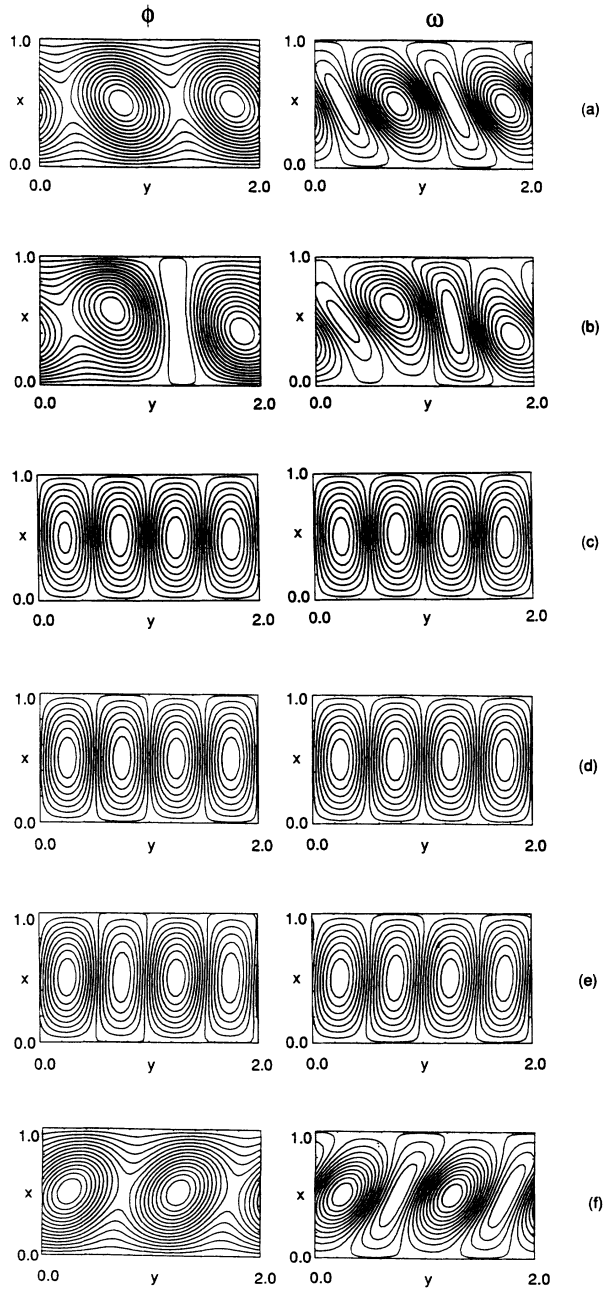

FIG. 9. Contours of the stream function and vorticity at (a) $t=600$, (b) $t=800$, (c) $t=960$, (d) $t=1080$, (e) $t=1120$, and (f) $t=1400$ for $\mu=2.1213\times10^{-3}$.

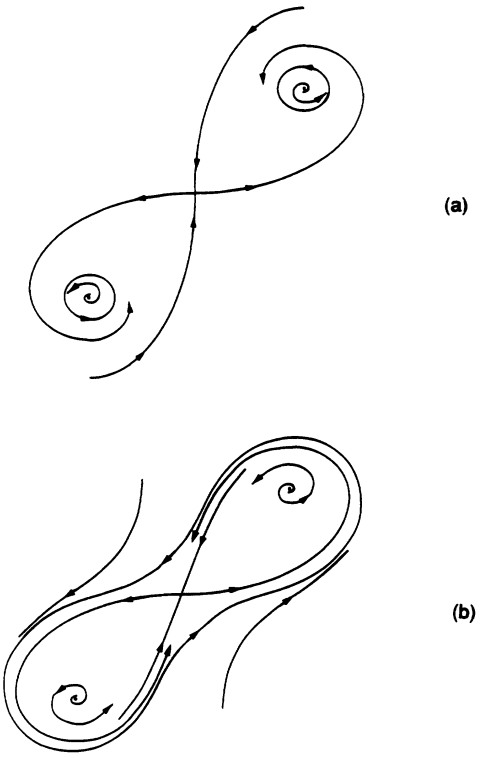

FIG. 10. Schematic phase portrait of the trajectory (a) before and (b) after global bifurcation.

evolved very close to a state reminiscent of a single island with shear flow (the difference, however, being the weak doublet structure at the center of the island due to the four-vortex driver). Such a state was the final steady state of the earlier work reported in Refs. [8] and [9]. However, in the present case the "orbit" is in the vicinity of this fixed point where it spends a significant time. Thus the presence of this fixed point affects the periodic orbit. This would suggest that any further reduction in the viscosity would lead to an inverse Hopf bifurcation, where a stable periodic orbit would go over to a stable fixed point with the change of the control parameter. This is precisely what is observed at $\mu=\mu_c=7.25\times10^{-4}$. As we decrease the viscosity, the period of the oscillations keeps increasing. The increase in the period scales as $T=(\mu-\mu_c)^{-0.25}$. This fixed point is like the state shown in Fig. 13. Except for the two small O points and X point at the center of the coalesced vortices, the general flow is similar to the steady-state solutions of the two-vortex study of Ref. [9], Figs. 6(c) and (d). However, in this case there are again four such degenerate states because of the inherent symmetry in the present system. A second such state would be one with a phase change of π, but with the same vorticity for the shear flow. Similarly there would be two more states for the shear flow with vorticity in the opposite direction.

The above-mentioned fixed point survives for a large window in viscosity until $\mu=4.0\times10^{-5}$. The fixed point or steady state becomes unstable and gives rise to a time-dependent chaotic state which is beyond the scope of the

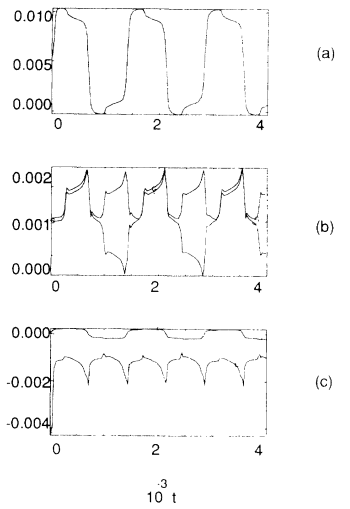

FIG. 11. For $\mu=7.50\times10^{-4}$, time history of the (a) $k_y=0$ Fourier component, sin (S) and cos (C) components for (b) $k_y=2\pi y/L_y$, and (c) $k_y=2\pi y/L_y$ of ϕ.

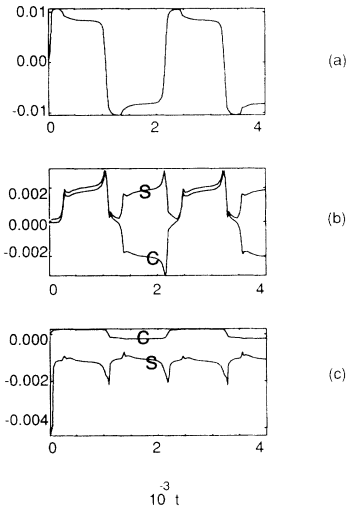

FIG. 12. For $\mu=7.3\times10^{-4}$, time history of the (a) $k_y=0$ Fourier component, sin (S) and cos (C) components for (b) $k_y=2\pi y/L_y$, and (c) $k_y=2\pi y/L_y$ of ϕ.

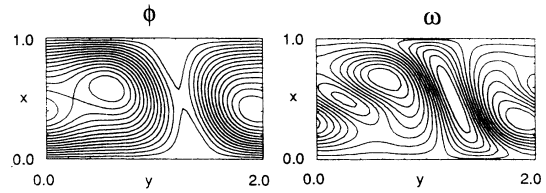

FIG. 13. Stream function and vorticity for $\mu=7.3\times10^{-4}$ at $t=500$. This is also the fixed point at $\mu=7.25\times10^{-4}$.

present work and which can be qualitatively understood in terms of low-dimensional dynamics.

IV. CONCLUSIONS

We have studied the nonlinear evolution of four alternately counterrotating vortices in a two-dimensional box with hard-wall free-slip boundary conditions in the x direction and periodic boundary conditions in the y direction. This study was motivated by earlier work of Refs. [8] and [9] to understand the generation of shear flow in two-dimensional fluids. Also, in recent experiments [3–7] the interaction of an array of electromagnetically driven counterrotating vortices has been studied.

As we vary the viscosity from 10^{-2} to 2.5×10^{-3} we observe a series of pitchfork bifurcations from a pure four-vortex state to a four-vortex state with shear flow, and finally to a state which is an admixture of a four-vortex state, a two-vortex state, and shear flow. The first bifurcation is caused by the shear flow instability studied earlier [8,9]. The second bifurcation is a consequence of the pairing instability [10–12]. These transitions are similar to the ones observed in the experiments.

Beyond this point, decreasing the viscosity gives rise to a supercritical Hopf bifurcation as the last fixed point goes unstable. This is followed by a global bifurcation at $\mu=2.1213\times10^{-3}$, which leads to periodic self-reversal of the shear flow. This global bifurcation is perhaps the most interesting feature of the present studies, because of the implications for geophysical and solar dynamo, where periodic reversal of magnetic fields is observed. Studying the dynamics of the magnetic field as a passive scalar in a fluid flow with periodic reversal of vorticity would be a natural extension of the present work.

A further decrease in the viscosity leads to an inverse Hopf bifurcation as the system evolves to a steady two-vortex state with shear flow, very similar to the nonlinear states obtained in the earlier work [8,9]. This state persists for a large window in the viscosity parameter space until $\mu=4\times10^{-5}$. Then follows a transition to temporal chaos. The various transitions are shown in Table I.

Many of these features are similar to the various transitions observed in the fluid experiments. However, it is difficult to make a direct comparison with the experiments because of the following reasons. The viscosity in our studies changed by a factor of 400 to observe the transition from the steady-state four-vortex case to the chaotic phase. However, we need to remind the reader that the Reynolds number changed only by a factor of 20. This is because as we went to lower viscosity the strength of the four-vortex component decreased. This can be readily seen by examining the magnitude of the four-vortex components in Figs. 3, 5, 7, 8, and 12, which correspond to decreasing μ. Quantitatively we find that $|v^{\max}|^2\propto\mu$. Thus the Reynolds number $R=v^{\max}/\mu\propto\mu^{-1/2}$.

The sequence of bifurcations observed in our simulations agrees well with the experiments up to the point where we get our first supercritical Hopf bifurcation. The existence of the global bifurcation, during which the shear flow reverses, was not reported in the experiments. The very strong symmetry that exists in the equations for

TABLE I. Transitions to temporal chaos.

Viscosity range	Nonlinear state
$\mu < 5.0\times10^{-3}$	Four-vortex steady state
$3.0\times10^{-3} < \mu < 5.0\times10^{-3}$	Four-vortex with shear flow steady state
$2.25\times10^{-3} < \mu < 3.0\times10^{-3}$	Four-vortex–two-vortex with shear flow steady state
$\mu = 2.25\times10^{-3}$	Supercritical Hopf bifurcation
$2.1213\times10^{-3} < \mu < 2.25\times10^{-3}$	Periodic state
$\mu = 2.1213\times10^{-3}$	Global bifurcation with self-reversal of shear flow
$7.25\times10^{-4} < \mu < 2.1213\times10^{-3}$	Periodic state with period $T(\mu-\mu_c)^{-0.25}$ and $\mu_c = 7.25\times10^{-4}$
$4.00\times10^{-5} < \mu < 7.25\times10^{-4}$	Dominantly two-vortex with shear flow steady state
$\mu < 4.00\times10^{-5}$	Quasiperiodic and temporally chaotic state

allowing shear flow to go either way is the reason why such self-reversals can occur. If, however, in the experiments there is a bias towards getting shear flow in one preferred direction, then a special effort has to be made to make sure that no preferential status for a particular vorticity for the shear flow exists. The transition to chaos observed by us appears to be a higher-dimensional process and not the period-doubling bifurcations observed in the experiments. A major difference between the numerical simulations and the experiments is the boundary condition in the y direction. We used periodic boundary conditions. In the experiment the fluid is free to flow in the regions beyond the outermost stirring magnets. The walls containing the fluid are significantly far away from the stirring region. For the four-vortex case, the difference in the boundary conditions in the y direction would be expected to be a major factor in causing the discrepancy between the numerical results and the experiments. We have done some preliminary work with eight vortices (for which the boundary conditions would be less important than the four-vortex case) and have indeed found bifurcations similar to the experimental ones. However, there is added dimension of richness to the eight-vortex case which gives rise to more varieties of bifurcations compared to the four-vortex case. In view of the complexity of the eight-vortex system, we have just reported the four-vortex study which could at least be qualitatively understood in terms of the shear flow and pairing instabilities. Finally the aspect ratio of the vortices used in our numerical work is unity. As stated earlier, this choice of the aspect ratio renders the inviscid mode stable. Choosing $L_y < 2.0$ would make the inviscid mode, which has a larger growth rate than the viscous mode, unstable. Of course this could change the various bifurcations as the viscosity is reduced. These studies will be pursued in the future.

ACKNOWLEDGMENT

This work was supported by the U.S. Department of Energy (MFE).

[1] E. R. Priest, in *Solar Magnetohydrodynamics* (Reidel, London, 1982), p. 15.
[2] S. Chandrashekar, *Hydrodynamics and Hydromagnetic Stability* (Oxford University Press, London, 1961), p. 9.
[3] J. Sommeria, J. Fluid Mech. **170**, 139 (1986).
[4] P. Tabeling, S. Fauve, and B. Perrin, Europhys. Lett. **4**, 555 (1987).
[5] P. Tabeling, S. Cardoso, and B. Perrin, J. Fluid Mech. **213**, 511 (1990).
[6] O. Cardoso, H. Williame, and P. Tabeling, Phys. Rev. Lett. **65**, 1869 (1990).
[7] H. Williame, O. Cardoso, and P. Tabeling, Phys. Rev. Lett. **67**, 3247 (1991).
[8] J. F. Drake, J. M. Finn, P. Guzdar, V. Shapiro, V. Shevchenko, F. Waelbroeck, A. B. Hassam, C. S. Liu, and R. Z. Sagdeev, Phys. Fluids B **4**, 488 (1992).
[9] J. M. Finn, J. F. Drake, and P. N. Guzdar, Phys. Fluids B **4**, 2768 (1992).
[10] H. Lamb, *Hydrodynamics* (Cambridge University Press, Cambridge, England, 1932), p. 221.
[11] M. V. Melander, N. J. Zabusky, and A. S. Styczek, J. Fluid Mech. **167**, 95 (1986).
[12] M. V. Melander, N. J. Zabusky, and J. C. McWilliams, J. Fluid Mech. **195**, 303 (1988).